Structure and Dynamics of an Amphiphilic Peptide in a Lipid Bilayer: A Molecular Dynamics Study

Katarína Belohorcová,* James H. Davis,* Thomas B. Woolf,§ and Benoît Roux#
*Department of Physics, University of Guelph, Guelph, Ontario N1G 2W1, Canada; #Départements de physique et de chimie, Université de Montréal, Montréal, Québec H3C 3J7, Canada; and §Department of Physiology, Johns Hopkins University School of Medicine, Baltimore, Maryland 21205 USA

ABSTRACT A molecular dynamics simulation of a simple model membrane system composed of a single amphiphilic helical peptide (ace-$K_2GL_{16}K_2A$-amide) in a fully hydrated 1,2-dimyristoyl-*sn*-glycero-3-phosphocholine bilayer was performed for a total of 1060 ps. The secondary structure of the peptide and its stability were described in terms of average dihedral angles, ϕ and ψ, and the C_α torsion angles formed by backbone atoms; by the average translation per residue along the helix axis; and by the intramolecular peptide hydrogen bonds. The results indicated that residues 6 through 15 remain in a stable right-handed α-helical conformation, whereas both termini exhibit substantial fluctuations. A change in the backbone dihedral angles for residues 16 and 17 is accompanied by the loss of two intramolecular hydrogen bonds, leading to a local but long-lived disruption of the helix. The dynamics of the peptide was characterized in terms of local and global helix motions. The local motions of the N-H bond angles were described in terms of the autocorrelation functions of $P_2[\cos \theta_{NH}(t, t + \tau)]$ and reflected the different degrees of local peptide order as well as a variation in time scale for local motions. The χ_1 and χ_2 dihedral angles of the leucine side chains underwent frequent transitions between potential minima. No connection between the side-chain positions and their mobility was observed, however. In contrast, the lysine side chains displayed little mobility during the simulation. The global peptide motions were characterized by the tilting and bending motions of the helix. Although the peptide was initially aligned parallel to the bilayer normal, during the simulation it was observed to tilt away from the normal, reaching an angle of ~25° by the end of the simulation. In addition, a slight bend of the helix was detected. Finally, the solvation of the peptide backbone and side-chain atoms was also investigated.

INTRODUCTION

It is now widely accepted that the biological function of proteins is inherently connected to their motion. Motion can occur on different time scales (ranging from femtoseconds to many hours), different length scales (from 0.01 Å up to 100 Å), and different energies (0.1–100 kcal/mol) (e.g., Brooks et al., 1988). Membrane proteins exist in a very complex environment, the composition of which varies immensely from organism to organism. The function of the membrane is not only to act as a semipermeable barrier, but also to maintain and facilitate the function and stability of membrane proteins (Stowell and Rees, 1995). In principle, spectroscopic techniques (i.e., vibrational or Raman spectroscopy, NMR spectroscopy, etc.) can be used to elucidate the nature of protein structure and dynamics in biological membranes. However, spectroscopic measurements provide information averaged over the time scale of the experiment. The fine details of the molecular motion are not directly measured if the motion is fast relative to the experimental time scale (Brooks et al., 1988; Gennis, 1989). More detailed information on molecular structure, dynamics, and energetics on an atomic level can be obtained by theoretical methods such as molecular dynamics (MD) (van Gunsteren and Mark, 1992). Because MD can, in principle, provide detailed information that is not easily accessible experimentally, it is a particularly powerful method for studying membrane proteins (Pastor, 1994). However, the bulk of the work in the field of MD consists of simulations of simple and complex liquids, proteins in vacuum or water, lipid monolayers and bilayers, DNA, etc., and it is only very recently that there has been progress in the study of membrane proteins. This paper concentrates on the investigation of static and dynamic properties of a peptide that is incorporated into a hydrated lipid bilayer, presenting a simple model of a biological membrane.

In MD, changes in atomic positions are obtained by solving Newton's equations of motion. The equations of motion are integrated in small time steps, thus producing individual atomic trajectories (Haile, 1992). From atomic trajectories a wealth of information can be obtained, e.g., time averages of different macroscopic properties, both static and dynamic, and time dependences of different processes (Haile, 1992). The MD method does have limitations, however. One of these limits is the use of an empirical potential function in which approximations and simplifications have been made to achieve a balance between computational efficiency and the accuracy of the potential function (Brooks et al., 1988). Furthermore, the short length of the simulation (currently reaching up to a nanosecond) and the small size of the system (which can comprise a few thousand atoms) limit the configurational sampling. Finally, the numerical integration of Newton's equations of motion requires the use of finite-difference methods that may be

Received for publication 17 January 1997 and in final form 21 August 1997.

Address reprint requests to Dr. James Davis, Department of Physics, Guelph University, Guelph, ON N1G 2W1, Canada. Tel.: 519-824-4120, X2659; Fax: 519-836-9967; E-mail: jhd@physics.uoguelph.ca.

0006-3495/97/12/3039/17 $2.00

imprecise because of truncation and round-off errors. Ultimately, the computational limitations are related to the current hardware.

Many MD simulations of proteins in vacuum or water (e.g., see Brooks and Karplus, 1989; Kovacs et al., 1995; Hirst and Brooks, 1995; van Gunsteren et al., 1995; etc.) and of lipid bilayers (e.g., see Pastor et al., 1991; Venable et al., 1993; Stouch, 1993; Heller et al., 1993, etc.) have now been performed. These simulations have shown the power of the method and thus pave the way for simulations of more complicated systems, such as biological membranes. However, MD simulations of biological membranes that include a protein embedded in a hydrated lipid bilayer are still rare, because of the lack of accurate experimental structures. Currently, relatively few three-dimensional structures of membrane proteins are known with high resolution, such as bacteriorhodopsin (Grigorieff et al., 1996), the photosynthetic reaction centers of *R. viridis* (Deisenhofer and Michel, 1989) and *R. sphaeroides* (Ermler et al., 1992), prostaglandin synthase (Picot et al., 1994), the light-harvesting complex II of photosystem II (Kühlbrandt et al., 1994), porin (Weiss and Schulz, 1992), and *Staphylococcus aureus* α-hemolysin pore (Song et al., 1996). All of these membrane proteins have a large molecular weight, and thus a conventional MD simulation of a model membrane containing such a membrane protein presents a major challenge. Additional difficulties are presented by the construction of the initial configuration of the simulation system. Thus far, a limited number of MD simulations of model membranes containing a transmembrane peptide have been reported. One of the earliest simulations was that performed by Edholm and Johansson (1987). They simulated a polypeptide α-helix inserted into a simplified model membrane composed of 16 carbon single-chain amphiphiles harmonically attached to a plane to maintain a bilayer configuration; no solvent water molecules were included. More recently, all-atom MD simulations followed: the gramicidin channel in a fully hydrated dimyristoylphosphatidylcholine (DMPC) bilayer (Woolf and Roux, 1994a, 1996), Pf1 coat protein in a dipalmitoylphosphatidylcholine (DPPC) bilayer (Roux and Woolf, 1996), a C-terminal fragment (residues 13–41) of human corticotropin-releasing factor in a dioleoylphosphatidylcholine bilayer (Huang and Loew, 1995), a model all-alanine α helix in DMPC (Shen et al., 1997), individual α-helices from bacteriorhodopsin in DMPC (Woolf, 1996), and melittin in a DMPC bilayer (S. Berneche and B. Roux, private communication). Edholm et al. (1995) performed an MD simulation of the native bacteriorhodopsin in purple membrane, using a united atom model. To our knowledge, this is the only MD simulation of a multihelix membrane protein in a lipid bilayer. A few simulations elucidating the diffusion mechanism of small molecules, such as benzene and 1,4-dihydropyridine calcium channel antagonist, and water transport through a lipid membrane, have been reported (Bassolino-Klimas et al., 1993, 1995; Alper and Stouch, 1995; Marrink and Berendsen, 1994). Furthermore, MD studies of the interaction of small peptides with a lipid bilayer have been performed (Damodaran et al., 1995; Damodaran and Merz, 1995).

The complexity of motions occurring in a biological membrane may ultimately require extended simulation periods with time scales of up to seconds. This is because the equilibration time of the system is longer than the longest intrinsic relaxation time of the system (van Gunsteren and Mark, 1992). Although it is not currently possible to perform a sufficiently long simulation to investigate such long time scales, we can still learn about the short-time-scale processes, provided that the system is stable. The duration of equilibration depends on how far the system in its initial configuration is from the equilibrium state (Haile, 1992). Therefore the choice of the initial configuration of the system is extremely important. One of the possible approaches to the construction of the initial configuration of a model membrane is the "overlay" method. This was used by Edholm and Johansson (1987) to build a system composed of a polypeptide α-helix and a simplified model membrane composed of 100 single-chain amphiphiles harmonically attached to a plane. No solvent water molecules were included. To construct the initial configuration, a number of chains were removed from a previously equilibrated lipid bilayer, and the helix was inserted into the created cavity. This method worked because of the simplicity of the model membrane, the absence of solvent water molecules, and the relatively regular shape of the α-helix. However, this method is inappropriate for inserting a protein of a more complicated shape into a fully hydrated membrane of phospholipids molecules with two hydrocarbon chains. A novel protocol designed by Woolf and Roux (Woolf and Roux, 1996; Roux and Woolf, 1996) allows the construction of more complicated systems. The basic idea is to assemble a system from individual preequilibrated components. The current system was constructed according to this method, starting with a synthetic peptide, prehydrated phospholipids, and bulk water molecules (Woolf and Roux, 1994b, 1996; De Loof et al., 1991; Pastor et al., 1991; Venable et al., 1993).

The MD simulation reported here used a transbilayer synthetic peptide (acetyl-Lys_2-Gly-Leu_{16}-Lys_2-Ala-amide) belonging to a class of extensively experimentally studied peptides with sequences ace-Lys_2-Gly-Leu_n-Lys_2-Ala-amide or ace-Lys_2-Leu_n-Lys_2-Ala-amide (these will be referred to as peptide-*n*, where *n* is the number of leucines in the hydrophobic part of the peptide, n = 16, 20, 24). The model membrane system consists of a fully hydrated DMPC bilayer into which peptide-16, including an acetylated N-terminus, was inserted. The system composition was chosen to correspond to samples studied experimentally (J. Qian and J. H. Davis, private communication). The structure of the peptide was chosen so that it would have an amphiphilic character, with a long hydrophobic core, and lysines at both termini interacting with the polar environment. Circular dichroism studies (Davis et al., 1983; Prosser et al. 1992) showed that peptide-*n* molecules adopt an α-helical conformation in a lipid bilayer. The synthetic peptide thus repre-

sents a very simple model of a membrane protein, because it is believed that the membrane-spanning domain of a membrane protein may generally consist of a single α-helical polypeptide or several structured strands of amino acids (Mouritsen and Bloom, 1993). The different length of the hydrophobic core was designed to study the effect of the mismatch of the hydrophobic regions of the peptide and the bilayer on the bilayer thickness (Nezil and Bloom, 1992). It was found that the average thickness of the lipid bilayers was significantly perturbed in cases of a large mismatch. Zhang et al. (1992a) studied the conformation and amide hydrogen exchange of peptide-24 dispersed in fully hydrated phospholipid bilayers by Fourier transform infrared spectroscopy. Their results indicate that at least 80% of the helix retains its α-helical conformation, which means that the entire polyleucine core of the peptide must be included in its α-helical domain. The hydrogen exchange experiments provide insight into the stability of α-helical conformations. The greater propensity for H/D exchange at both peptide termini may indicate reduced stability of the α-helical conformation at these ends. X-ray diffraction experiments were performed on systems composed of peptide-16 and peptide-24, respectively, inserted in a DPPC bilayer in a gel phase (Huschilt et al., 1989). The lipid:peptide mole ratio of the former was 10:1, and that of the latter was 30:1. The conclusions were that the helices oriented themselves with their helical axes perpendicular to the lipid bilayer to within 25°. A NMR dynamics study of the backbone of peptide-24 in a DPPC bilayer was performed by Pauls et al. (1985) at different temperatures, both in the gel state and in the liquid-crystalline state of the bilayer. The results showed that the average angle between the motional symmetry axis and the N-^{2}H bond was close to 19° in a liquid crystalline state bilayer at 42°C. The correlation time of the fast reorientational motion about the helix axis was found to decrease with increasing temperature.

In the next section, the basic steps of the system construction are described. Then the computational details are given, after which the equilibration and, finally, the simulation are described in detail. The structure of the peptide and its stability were investigated and, when possible, compared to experimental results. Local and global helix motions were analyzed to elucidate the nature and the time scales of the peptide motions within the length of the simulation. The local motions studied include, for example, the dynamics of the NH bonds and isomerizations of the side-chain dihedral angles. The global motions of the helix were investigated in terms of the tilt angle of the helix axis with respect to the bilayer normal (z axis) and of the bend angle of the helix.

MODEL AND METHODS

Construction of the initial configuration

The membrane system for the MD simulation consists of a synthetic peptide of the following sequence: acetyl-Lys_2-Gly-Leu_{16}-Lys_2-Ala-amide, 12 DMPC molecules (6 in each layer), and 593 water molecules, corresponding to a total of 3613 atoms. This is 51% water by weight. The total charge of the system was +4; however, counterions were not included in the system, because of the slow time scale (on the order of nanoseconds) of ion redistribution in solution (van Gunsteren et al., 1995). Molecular mechanics software CHARMM (Brooks et al., 1983) and the all-atom force field PARAM 22 (Mackerell et al., 1992) were used to build the system and to perform the MD simulation. The system was constructed using a protocol designed and described in detail by Woolf and Roux (1996) and in Roux and Woolf (1996, Ch. 17). The basic idea of the method is to construct the system in a state that is as close as possible to the equilibrium state of the bilayer in the liquid-crystalline phase, to avoid a lengthy heating and equilibration period.

The peptide was constructed in an ideal right-handed α-helical conformation because experiments have indicated that the peptide adopts this conformation in lipid bilayers (Davis et al., 1983; Huschilt et al., 1989; Prosser et al., 1992). The helix axis, aligned along the z direction, was parallel to the bilayer normal. The peptide was then energy minimized. The dihedral angles of the side chains were harmonically constrained to their optimal values obtained from the backbone-dependent rotamer library for proteins (Dunbrack and Karplus, 1993), the constraining force constants being 50 kcal/mol · rad^2}. The peptide backbone as well as C^β and C^γ atoms of the side chains were initially held fixed. Later they were constrained by a harmonic potential to their reference positions. The force constant of 5.0 kcal/mol · Å^2 was used first, and then a force constant of 1.0 kcal/mol · Å^2 was applied. Between changes in the force constant on the selected atoms, the peptide structure was energy minimized for 200 steps by the adopted basis-set Newton-Raphson (ABNR) method (Brooks et al., 1983). Finally, all of the constraints were removed and the peptide was energy minimized for another 300 steps by the ABNR method.

In the next stage the cross-sectional area of the system was determined. Because the simulation was performed with a constant number of particles (N) and under constant volume (V) and constant energy (E) conditions, the cross-sectional area of the system had to be determined with great care, as it has a direct influence on the state of the system (Woolf and Roux, 1996). The cross-sectional area of the peptide was calculated in the following manner. The total volume occupied by peptide atoms was found by searching through a set of grid points for points outside the van der Waals radius of any atom. By dividing the total occupied volume by its length, the mean cross-sectional area of the peptide was determined to be 173.5 Å^2. The number of lipids surrounding the peptide in each half of the bilayer was chosen to be six for symmetry reasons, and so that there would not be any large gaps between molecules. The average cross-sectional area per lipid was assumed to be 64 Å^2 (Gennis, 1989; Nagle, 1993). The cross-sectional area of the whole system was calculated to be 557.5 Å^2, defining the

area of the primary cell with the peptide placed in its center. Hexagonal periodic boundary conditions in the *xy* plane were imposed on the system. The horizontal distance d within the *xy* plane between the centers of neighboring cells was calculated to be 25.4 Å, using the expression

$$d = \sqrt{\frac{4}{3} A \cos 30^\circ} \quad (1)$$

where A is the area of the primary cell.

The system was then assembled from its individual components. To determine initial positions of the lipids, the peptide was surrounded with large van der Waals spheres, each with a cross-sectional area equal to that of one lipid. The spheres were constrained to remain in the *xy* planes at $z = \pm 14$ Å. They were allowed to rearrange themselves around the peptide during 10 ps of Langevin dynamics at 600 K, followed by 100 steps of ABNR energy minimization. Their positions in the *xy* plane determined the starting *x* and *y* coordinates of the glycerol C_2 carbons of the lipid molecules. Twelve lipids were then randomly chosen from a library of 2000 different lipid conformations. This set of lipid conformations was previously generated by a biased Monte Carlo sampling procedure of an isolated DPPC molecule in a mean field, the parameters of which were empirically adjusted so that the conformationally averaged orientational order parameter, S_{CD}, would be consistent with experimental values at 323 K (De Loof et al., 1991; Pastor et al., 1991; Venable et al., 1993). The lipid molecules were preequilibrated and prehydrated by ~20 water molecules, and the two last methylene groups were deleted to obtain a DMPC molecule whose chains are shorter by two carbons compared to a DPPC molecule (Woolf and Roux, 1994b, 1996). Because of the randomness of selected lipid conformations, many core-core overlaps between nonhydrogen heavy atoms were present in the system (i.e., some nonhydrogen atoms were closer to each other than 2.6 Å). These overlaps were removed by systematic rotations of the lipids (with their primary water molecules) and of the peptide by 10° about the *z* axis, followed by translation of lipids along the grid points in the *xy* plane. The system was then energy minimized by the steepest descent minimization method over 16 cycles, during which the van der Waals radius of the atoms was gradually increased to its full value. During this minimization the peptide was fixed and the C_2 atoms of the phospholipid glycerol were constrained to remain in the *xy* planes at $z = \pm 14$ Å.

In a final step, an equilibrated hexagonal box of 3888 water molecules was overlaid on the system, and water molecules lying in the hydrocarbon region defined to extend from $z = 11$ Å to $z = -11$ Å (Lewis and Engelman, 1983) and those within 2.6 Å of lipid or peptide atoms were deleted. The TIP3P water model was employed (Jorgensen, 1981; Jorgensen et al., 1983). The length of the primary cell was determined to be 68 Å, to give the desired level of hydration. Hexagonal images in the *xy* plane were translated by this amount in the *z* direction, resulting in an infinite multilayer system. After this the whole system was energy minimized for 200 steps by the ABNR method, while the peptide backbone was held fixed and the C_2 atoms of glycerol were constrained by planar harmonic constraints at $z = \pm 14$ Å. The resulting structure was the starting point for the equilibration.

Computational details

The equilibration and the simulation were performed in an *NVE* ensemble. The integration step was 2 fs, because the lengths of bonds containing hydrogens were constrained to a fixed value by SHAKE (Ryckaert et al., 1977). Nonbonded interactions were calculated by using a group-based cutoff (Brooks et al., 1983) with a switching function and were updated every 5 time steps. The switching function was turned on at 10 Å and turned off at 12 Å; no nonbonded interactions were calculated beyond 13 Å. The dielectric constant was set at 1.0. Atom coordinates were saved every 50 fs throughout the trajectory production period.

Equilibration

The equilibration for a total of 190 ps was performed in three stages. For the first 50 ps the system was weakly coupled to a heat bath by using Langevin dynamics to speed up the approach to equilibrium (throughout the rest of the equilibration the Verlet algorithm (Verlet, 1967) was used). The friction coefficient was small (3.0 ps^{-1}) to encourage movement (Loncharich et al., 1992). During the first 25 ps of this period, the peptide backbone was fixed and the C_2 atoms of glycerol were constrained by planar harmonic constraints at $z = \pm 14$ Å. For another 25 ps, the peptide backbone was harmonically constrained with a force constant equal to 2.0 kcal/mol · $Å^2$, and the force constant of planar harmonic restraints on the C_2 atoms of glycerol was decreased from 10.0 kcal/mol · $Å^2$ to 1.0 kcal/mol · $Å^2$. The temperature of the heat bath was 300 K for this stage. In the following 50 ps of equilibration, the temperature was set at 325 K to be well above the gel-to-liquid crystal transition point for DMPC (the phase transition temperature for DMPC is 24°C; Gennis, 1989). The constraints on the selected atoms were gradually removed, and the velocities were rescaled by a single factor when the temperature deviated by more than ±5 K from the equilibration temperature. For 25 ps the temperature was checked every 0.5 ps, and for the next 25 ps it was checked every 2.5 ps. Then the system was further equilibrated for 90 ps. The center of mass of the peptide was constrained by a cylindrical potential with a force constant of 10.0 kcal/mol · $Å^2$ to the origin of the coordinate system placed in the bilayer center. During this period, the system temperature was increasing; therefore a weak coupling to a heat bath by Langevin dynamics was used twice for a total of 15 ps to recover the original equilibrium temperature of 325 K. The coupling to the heat

bath was weak in both cases, with a friction coefficient of 0.5 ps^{-1}.

Simulation

The total length of the simulation (i.e., the trajectory production) was 1060 ps. The Verlet algorithm (Verlet, 1967) was used throughout the production run. The simulation was performed at a temperature of 325K. The center of mass of the peptide was restrained by a spherical potential to the origin of the coordinate system placed in the center of the simulation cell with a force constant of 1.0 kcal/mol · $Å^2$. No coupling to a heat bath was imposed on the system during the simulation. To determine whether the system was in equilibrium, the total energy, its decomposition into kinetic and the potential energies, and the temperature of the system were monitored throughout the equilibration and the simulation. Even though the simulation was performed in the microcanonical ensemble (i.e., at constant N, V, and E), the total energy was observed to gradually increase, in a stepwise fashion, with fairly long periods at a constant value. The increase in the total energy over the whole simulation represented an overall change of 10%. Both the kinetic and the potential energies contributed to the increase in the total energy. The kinetic energy increase may be due to the finite time step size (2 fs), to the accumulation of numerical and round-off errors, or to the choice of an *NVE* rather than a constant pressure simulation system (see Pastor and Feller, 1996). The resulting average temperature of the simulation was 335.5 K, with a root mean square (rms) deviation of 9.4 K. Despite the slow drift of the temperature, the calculated properties should be characteristic of a system at a temperature of 336 ± 9 K.

Analysis of results

CHARMM facilities and our own programs were used to analyze the results.

Determination of the helix axis

To determine the orientation of the helix axis for every saved coordinate set (each 50 fs), the following procedure was employed. The moment of inertia tensor of the peptide was calculated in a coordinate system with its origin placed at the center of mass of the peptide. The tensor was then diagonalized, and its eigenvalues and eigenvectors were calculated. Principal axes and principal moments of inertia were determined, and the helix axis was identified as the principal axis corresponding to the smallest eigenvalue (i.e., to the smallest principal moment of inertia).

Normalized autocorrelation function

The normalized autocorrelation estimate r_{xx} of a discrete time series $x(k)$, where $k = 0, 1, \ldots, N$, was calculated as follows (Jenkins and Watts, 1968):

$$r_{xx}(k) = \frac{c_{xx}(k)}{c_{xx}(0)} \tag{2}$$

where

$$c_{xx}(k) = \frac{1}{N}\sum_{t=1}^{N-k}[x(t) - \bar{x}][x(t+k) - \bar{x}] \tag{3}$$

and $\bar{x} = \sum_{k=1}^{N} x(k)$ is the sample mean of the whole series.

Radial distribution function

A convenient tool for investigation of the solvation of specified atoms and of the local structure of water around selected atoms is the radial distribution function $g_{ij}(r)$:

$$g_{ij}(r) = \frac{\Delta N(r)}{\rho_i \Delta V(r)} \tag{4}$$

where

$$\Delta V(r) = \frac{4\pi}{3}((r + \Delta r)^3 - r^3)$$

$\Delta N(r)$ is the number of molecules i in a spherical shell of thickness Δr, r is the distance between the molecule j and the spherical shell, and ρ_i is the bulk density of molecules i. The radial distribution function gives the probability of finding a molecule of type i around a molecule of type j. It is the ratio of a local density $\rho_i(r)$ of the molecules of type i (e.g., solvent) around a specified atom j to the system density ρ_i (Haile, 1992).

The molecular dynamics simulation and analysis of results were performed on a Silicon Graphics Challenge XL computer and on an IBM Risc 6000 workstation. One picosecond of the simulation required ~1.1 h of CPU time. The equilibration and the simulation took nearly 7 months.

RESULTS AND DISCUSSION

Structure of the peptide and its stability

It has been shown by circular dichroism experiments that the synthetic peptide-16 adopts an α-helical conformation in lipid bilayers (Davis et al., 1983; Huschilt et al., 1989; Prosser et al., 1992). Therefore, the peptide secondary structure and its stability were carefully examined and compared to available experimental data.

Backbone dihedral angles

Important factors determining the type of secondary structure adopted by the peptide are the backbone dihedral angles: ϕ, ψ, and the C_α torsion angles (the $C_{\alpha i}$ torsion angle was defined by four consecutive C_α atoms, starting at the ith residue). For an ideal α-helix, ϕ and ψ values are near −57° and −47°, respectively (Cantor and Schimmel, 1980); C_α

torsion angles are ~50° (Ramakrishnan and Soman, 1982). Fig. 1 shows average dihedral angles ϕ_i, ψ_i, and $C_{\alpha i}$ torsion angles and their rms deviations for every amino acid residue. A detailed analysis shows that residues 6–15 retain an α-helical structure, ϕ_i angles fluctuate about −64°, ψ_i angles fluctuate about −43°, and $C_{\alpha i}$ torsions about 48°. The rms deviations of both the ϕ and the ψ angles in the stable region of the helix (i.e., from residue 6 to residue 15) are ~10°. The dihedral angles at both ends of the peptide exhibit rms deviations that are ~1.5 times larger than those in the stable region of the α-helix, suggesting the deformation of the α-helix, as will be demonstrated later.

From the knowledge of ϕ and ψ time series, Ramachandran maps can be constructed showing unambiguously the type of the structure adopted by the peptide and its stability. The data points for the Ramachandran maps were collected every 5 ps over the whole trajectory. The plots (not shown) confirmed that the α-helical structure was well preserved for amino acid residues 4–15 and for residue 18. The Ramachandran data for the first three and for the last three amino acid residues were scattered over a large region, suggesting deviations from the regular α-helical structure. This effect was most pronounced for the glycine residue, which is known to be a helix breaker. An interesting change in the conformation was observed for Leu[17] (see Fig. 2 *a*). In its Ramachandran map, two distinct regions were occupied. The graphs of the evolution of angles ϕ_{17} and ψ_{17} (Fig. 2, *b* and *c*) show a correlated change of both angles toward lower values. The time dependence of the backbone dihedral angles of the neighboring residues, 16 and 18, was examined to see if the conformational change at Leu[17] was propagated along the peptide backbone. Concerted changes

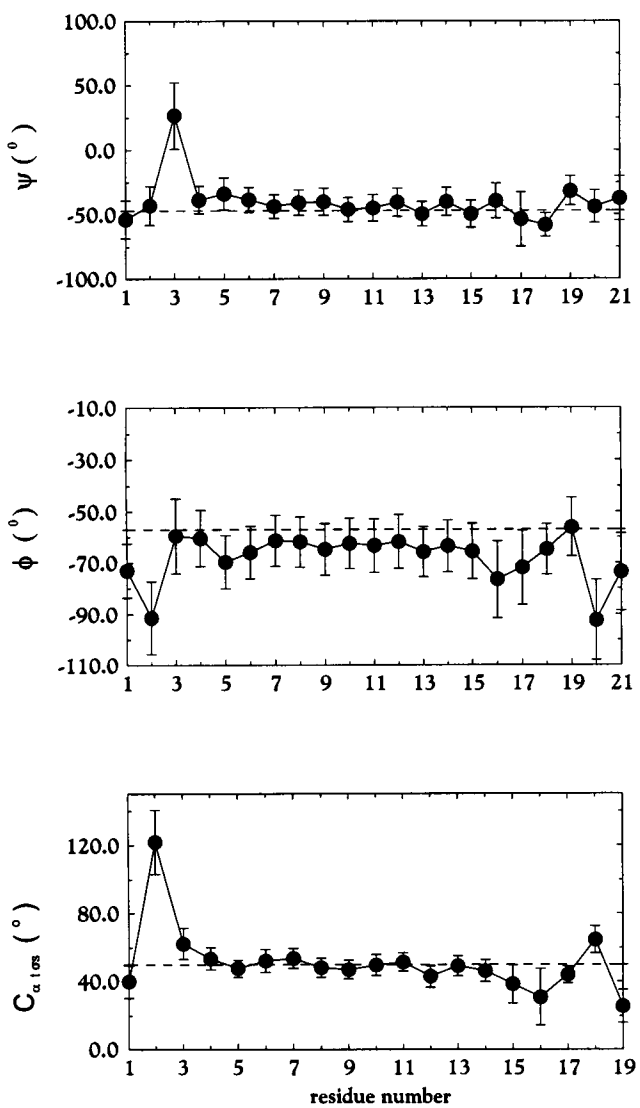

FIGURE 1 The average dihedral angles ϕ, ψ and C_α torsions versus residue number. Error bars were obtained from the rms deviations. Dashed lines denote the values typical of an ideal α-helix.

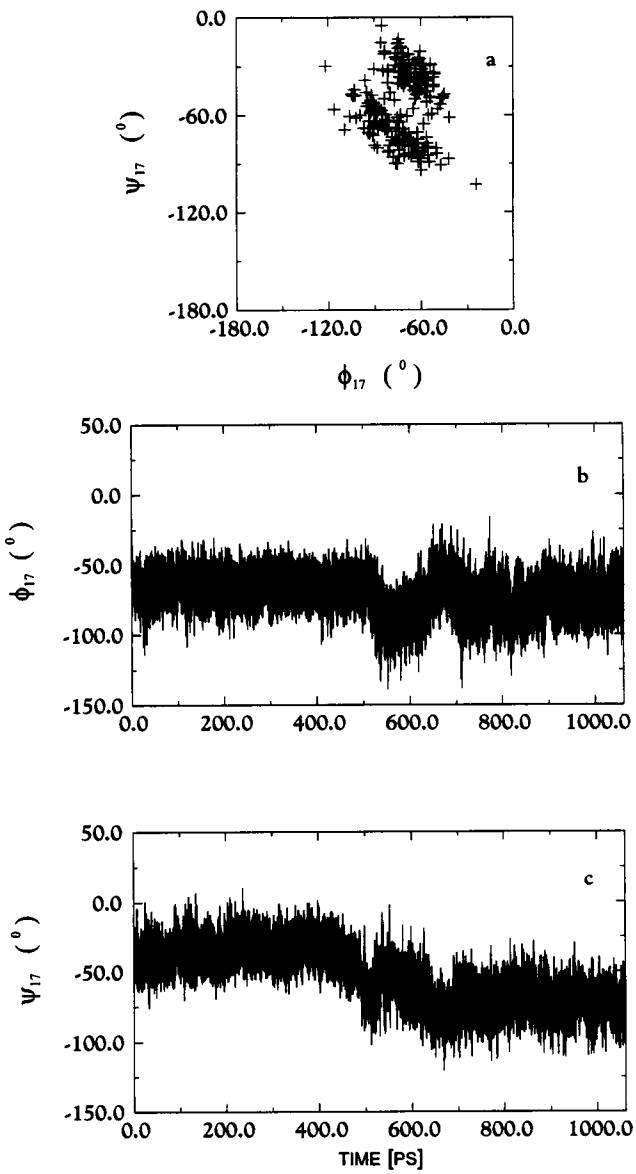

FIGURE 2 (*a*) The Ramachandran map of Leu[17]. (*b*) The evolution of the ϕ_{17} dihedral angle. (*c*) The evolution of the ψ_{17} dihedral angle.

in ϕ_{16} and ψ_{16} were observed (ψ_{16} toward higher values), whereas ϕ_{18} and ψ_{18} appeared to be affected only very slightly. Further analysis (see below) showed that this conformational change in backbone dihedral angles ϕ and ψ at leucines 16 and 17 was correlated with the breaking of hydrogen bonds in this region of the helix, amounting to a correlated deformation of the corresponding helix turn.

NH bond angles

Pauling and Corey (1951), in their work on the structure of synthetic polypeptides, predicted that, in an ideal right-handed α-helix, NH bond angles deviate 20° from the helix axis on average. To compare the simulation results to an ideal case, the time averages of NH bond angles with respect to the helix axis were calculated for all amino acid residues (the helix axis for the every saved coordinate set was calculated as indicated in Model and Methods). The average angles for residues 5–19 (see Fig. 3) fluctuated about 157° (or 180° − 157° = 23°), in good agreement with the expected value. However, angles at both termini, especially those at the N-terminus, exhibit large deviations from the predicted values, thus indicating that the first and the last turn of the peptide may not be in an α-helical conformation. From the knowledge of the NH bond angles with respect to the helix axis, θ_{NH}, one can calculate $\langle P_2[\cos(\theta_{NH})]\rangle$ for every amino acid residue. This variable is directly proportional to the deuterium quadrupolar splitting of a particular amino acid residue of the peptide. Consequently, the ^{2}H NMR spectrum of the peptide can be calculated and compared to the experimental spectrum. However, it should be emphasized that the time scale of the ^{2}H NMR technique is on the order of microseconds, whereas the molecular dynamics simulation covers only 1 ns, and thus care must be taken when comparing the two spectra.

Deuterium NMR experiments performed by Pauls et al. (1985) on a very similar system composed of peptide-24 dispersed in liquid-crystalline DPPC at 50°C agree well with the simulation results. The experiments determined, by analysis of ^{2}H NMR spectra, the angle between the axis of rotation (i.e., the helix axis) of the peptide and the N-^{2}H bond direction to be ~19°. Further analysis indicated a slight weakening of the α-helical conformation by the increased width of the edges of the spectrum at 50°C. Poor signal-to-noise did not allow further investigation of this point in a quantitative manner.

Deviation from ideal α-helical conformation

To investigate the unwinding and a possible bend of the helix backbone, the average projections of the $C_{\alpha i}C_{\alpha i+1}$ vectors on the helix axis were calculated and compared to the values typical of an ideal α-helix (see Fig. 4). The absolute value of the projection of the $C_{\alpha i}C_{\alpha i+1}$ vector is equivalent to translation along the helix axis for each residue. In an ideal α-helix this translation is equal to 1.5 Å (Brooks et al., 1988). At the N-terminus the average projection of the $C_{\alpha 1}C_{\alpha 2}$ vector is about −1 Å with an rms deviation of 0.7 Å, suggesting large fluctuations. Its negative value implies that this segment, at the N-terminus, is bent and pointing toward the bilayer interior instead of pointing outward, as expected of an α-helix. For the next three residues, the average projections are larger than 1.5 Å, indicating an extension, or stretching, of the helix backbone in this region. From residues 6 to 16 the average projection fluctuates around the value of ~1.5 Å, between 1.0 Å and 1.75 Å with fairly constant rms deviation. The value of the projection of the $C_{\alpha 18}C_{\alpha 19}$ vector is 0.32 Å, with a large rms deviation of 0.65 Å. A closer analysis of the time evolution showed a shortening of the peptide after 500 ps of the simulation, which was correlated with a conformational change in the backbone dihedral angles of Leu^{16} and Leu^{17}. In the first 500 ps, the average projection of the $C_{\alpha 18}C_{\alpha 19}$ vector on the helix axis was 0.91 Å ± 0.32 Å, whereas it

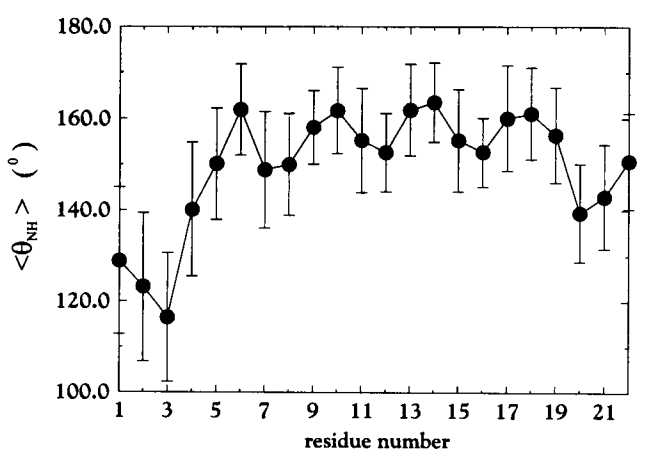

FIGURE 3 The average NH bond angles with respect to the helix axis versus residue number. Error bars were obtained from the rms deviations.

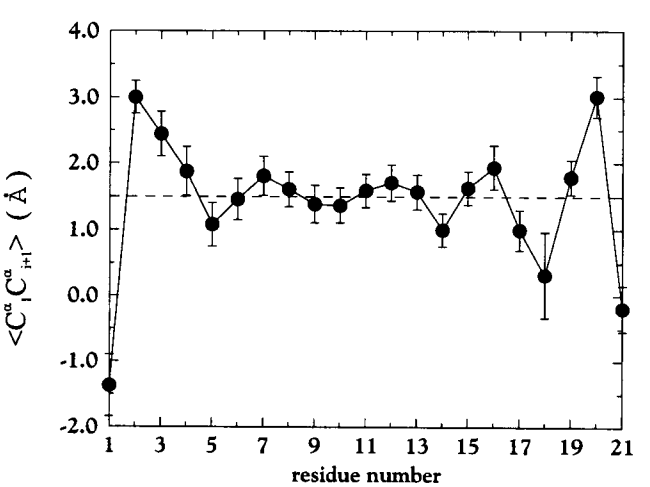

FIGURE 4 The average length of projection of $Ci^{\alpha}Ci + 1^{\alpha}$ vectors on the helix axis versus residue number. Error bars were obtained from the rms deviations. The dashed line denotes the value typical of an ideal α-helix.

was -0.22 Å $\pm$ 0.32 Å for the rest of the simulation. In addition, the average projection of the neighboring $C_{\alpha 17}C_{\alpha 18}$ vector is 1.0 Å $\pm$ 0.3 Å (i.e., shorter than expected). Finally, the last segment, at the C-terminus, is unwound and pointing toward the bilayer interior, but to a smaller extent than that at the N-terminus.

A possible extension of the peptide terminal residues was observed by Zhang et al. (1992a) in their FTIR experiments of the peptide-24 embedded in a DPPC lipid bilayer. They found that the peptide was predominantly in an α-helical conformation (its α-helical domain included the entire polyleucine core) and observed some non-α-helical structures, possibly in an extended conformation. Similar results were obtained for the shorter peptide-16.

Intramolecular peptide hydrogen bonds

An important characteristic of the α-helical structure is the hydrogen bonds between oxygens and amide hydrogens located four residues below (Pauling and Corey, 1951). They are thought to be a primary stabilizing factor for the secondary structure. Analysis of the existence and duration of these peptide intramolecular hydrogen bonds can be used to examine the stability of the peptide structure. The hydrogen bond between O_i and amide H_{i+4} was taken to exist if the atoms were closer to each other than 2.5 Å and if the oxygen-hydrogen-nitrogen angle was greater than 135° (Kovacs et al., 1995). Using this definition of hydrogen bond occurrence, it was determined that oxygens of residues 4–14 and of residue 18 were hydrogen bonded to their respective hydrogens for at least half of the total simulation. In contrast, the oxygen of Leu^{17} stayed hydrogen bonded to the amide hydrogen of Lys^{21} for only 12% of the simulation time. The average distances between the oxygens and the amide hydrogens four residues down the helix are shown in Fig. 5. The first two oxygens do not hydrogen bond with the peptide hydrogens at all, because their average distance is larger than 2.5 Å for every saved configuration, reflecting the fact that part of the first turn of the helix is extended. Instead of forming a regular $i \rightarrow i + 4$ bond, O_1 was hydrogen bonded to H_4 for 4.3% of the simulation time and O_2 was hydrogen bonded to H_4 for 15.7% of the simulation time (O_1 and O_2 occupy, on average, the same z region, because of the bend of the backbone at the N-terminus). O_3 was hydrogen bonded to H_7 and to H_6 as well, for 6.8% and 24.1% of the simulation time, respectively. This arrangement of the hydrogen bonds is typical of the 3_{10}-helix, with $i \rightarrow i + 3$ intramolecular hydrogen bonds. This helical conformation has been observed at the ends of α-helices, where one helix turn might have this conformation locally (Creighton, 1983).

To judge the stability of the helix, the number of intramolecular hydrogen bonds was calculated (see Fig. 6). In a 22-residue-long ideal α-helix, the number of intramolecular hydrogen bonds is 18. The maximum number of hydrogen bonds observed in the present case is 16, because the two lysine oxygens at the N-terminus do not participate in

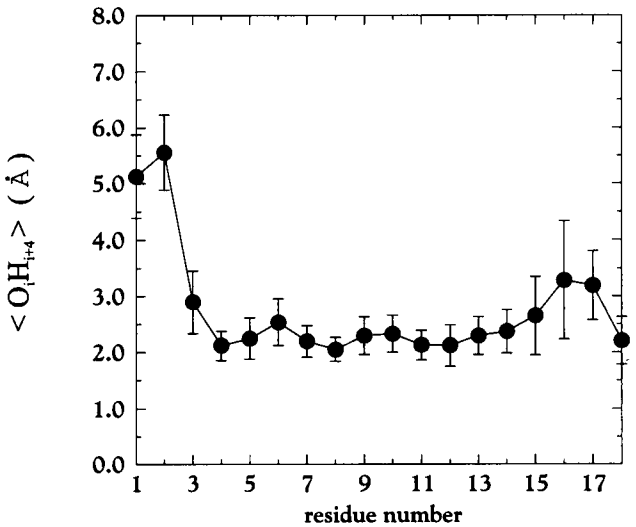

FIGURE 5 The average distances between an oxygen of ith residue and an amide hydrogen of i + 4th residue. Error bars were obtained from the rms deviations.

peptide intramolecular hydrogen bonds, as was discussed above. At ~500 ps into the simulation, it can be seen that on average another two hydrogen bonds were lost (Fig. 6). The loss of these hydrogen bonds was caused by a correlated increase in $O_{15}H_{19}$ and $O_{16}H_{20}$ distances that occurred at ~500 ps. Closer investigation showed that the $i \rightarrow i + 4$ hydrogen bond was replaced by an $i \rightarrow i + 5$ hydrogen bond in the case of O_{15}. H_{19} thus became free to hydrogen bond to another oxygen, namely to O_{14}, which hydrogen bonded to either H_{19} or to H_{18}, or possibly to both of them at the same time for very short periods of time during the second

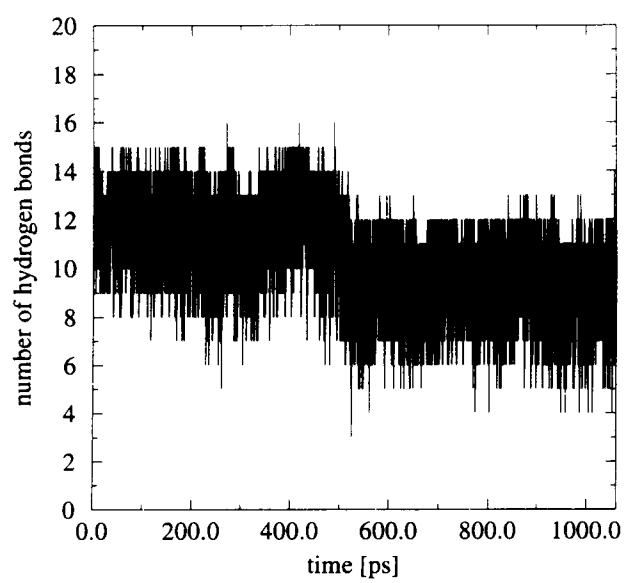

FIGURE 6 The evolution of the number of intramolecular hydrogen bonds stabilizing the α-helix. A hydrogen bond was defined to exist if the oxygen-hydrogen distance was less than 2.5 Å and if the nitrogen-hydrogen-oxygen angle was larger than 135° (Kovacs et al., 1995).

half of the simulation. This is directly correlated to the shortening of the projection of $C_{\alpha 18}C_{\alpha 19}$ vector on the helix axis, thus bringing H_{19} closer to O_{14}. The breakage of the $O_{15}H_{19}$ bond and the formation of new hydrogen bonds between O_{15} and H_{20} and between O_{14} and H_{19} are shown in Fig. 7. The time evolution of the O_iH_{i+4} distance illustrates the duration of this hydrogen bond; its breakage and its subsequent reformation are reflected in changes in O_iH_{i+4} distance. The breakage of the hydrogen bonds discussed earlier is closely connected to the conformational change of the helix backbone between Leu^{16} and Leu^{17} (see Fig. 2) and to the helix deformation between Leu^{17} and Leu^{19}.

When all of the results concerning the helix stability are considered, it is concluded that, on the average, residues 6–15 retain their α-helical conformation, whereas both helix ends exhibit more flexibility. There appears to be a long-lived disruption of the α-helix at residues 16 and 17 midway through the simulation, resulting in the breakage of two hydrogen bonds and a deformation of the corresponding helix turn.

Finally, the average distance between the carbonyl carbon of Leu^8 and the α carbon of Leu^{11}, and the distance between the carbonyl carbon of Leu^{11} and the α carbon of Leu^{12} were calculated and compared to experimental data (Langlais, 1994). The experimental distance r between labeled atoms was determined from ^{13}C NMR experiments through the internuclear dipolar coupling D_{ij}^{α}, which is proportional to $1/\langle r_{ij}^3 \rangle$, as follows:

$$r = \left\langle \frac{1}{r_{ij}^3(t)} \right\rangle^{-1/3} \tag{5}$$

where $r_{ij}(t)$ is the distance between the labeled atoms i and j, and the brackets denote the time average over the experimental time scale. To be consistent with the experimental determination of distances between the labeled atoms, Eq. 5 was used to evaluate the distances instead of direct calculations. The simulation results and the experimental values are in good agreement, as shown in Table 1.

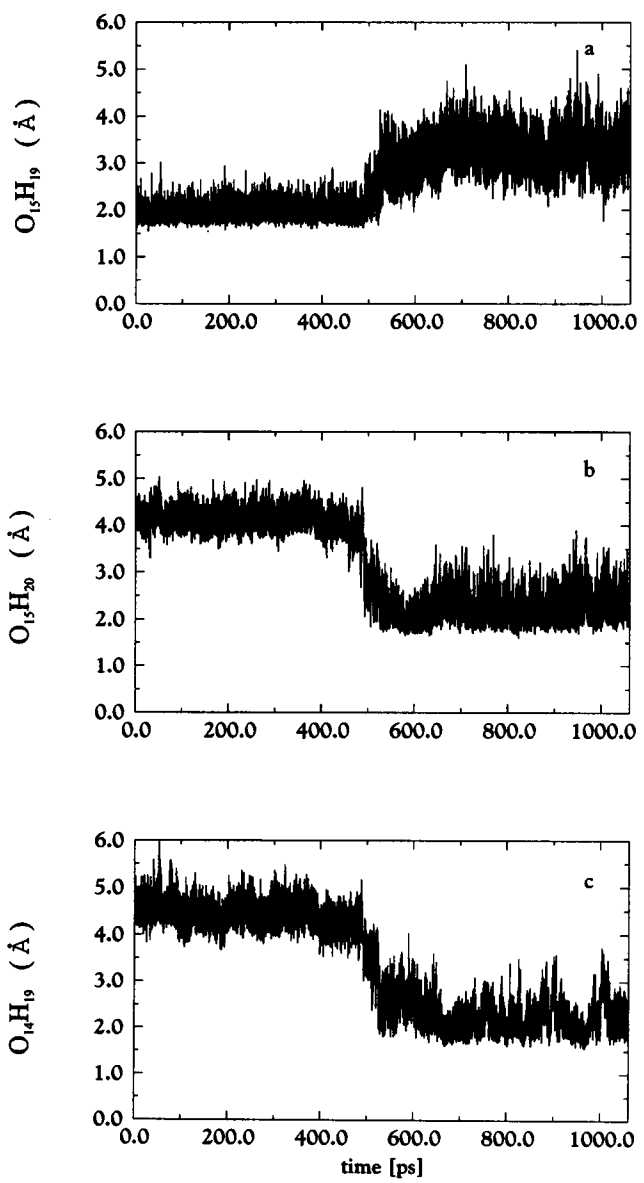

FIGURE 7 Illustration of (*a*) the breakup of $O_{15}H_{19}$ hydrogen bond after ~500 ps of the simulation. At the same time, a new hydrogen bond is possibly formed between O_{15} and H_{20} (*b*) and between O_{14} and H_{19} (*c*).

Dynamics of the peptide

Local peptide motions

Dynamics of NH bonds

Molecular dynamics simulations can provide information complementary to NMR experiments, even though the time scales of the two methods differ by several orders of magnitude. The details of the N^2H bond motion that are not obtainable from experiment (because the ^2H NMR spectrum of the peptide reflects the averaged motion of the N^2H bond angles over the time scale of the experiment) can be studied in detail by molecular dynamics. In the simulation, amide hydrogen was used instead of deuterium; however, the behavior of the N^2H bond motion is expected to be similar to that of the NH bond.

The motion of NH bonds was determined in terms of autocorrelation functions of $P_2[\cos \theta_{NH}(t, t + \tau)]$, where $\theta_{NH}(t, t + \tau)$ is the difference in NH bond angle with respect to the helix axis at times t and $t + \tau$. In Fig. 8 the autocorrelation functions of $\theta_{NH}(t, t + \tau)$ for three different residues are shown, providing a representative sample of autocorrelation functions obtained for all amino acid residues. The autocorrelation function of the first residue consists of two parts, a very fast initial decay followed by a

TABLE 1 The experimental and calculated distances between the labeled atoms

Atoms	Experimental values (Å)	Simulation results (Å)
C_8 $C_{\alpha 11}$	4.5 ± 0.3	4.6 ± 0.2
C_{11} $C_{\alpha 12}$	2.1 ± 0.2	2.5 ± 0.1

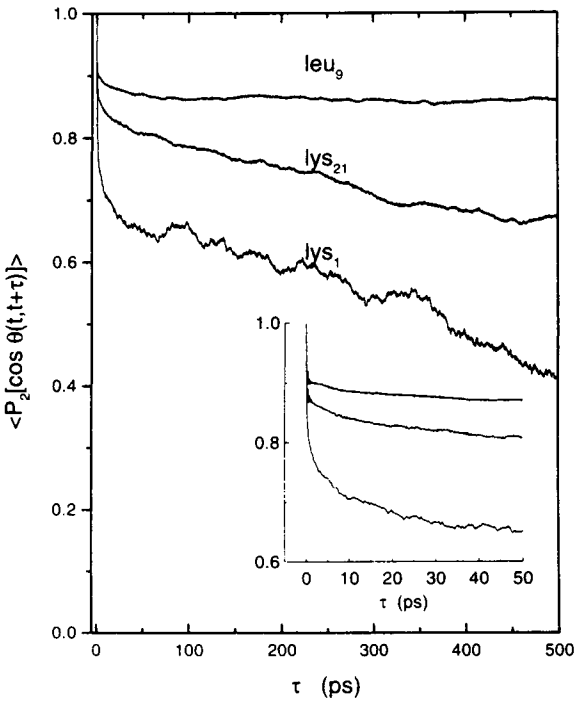

FIGURE 8 Autocorrelation functions of $P_2[\cos \theta_{NH}(t, t + \tau)]$ for Lys^1, Leu^9, and Lys^{21}. These three autocorrelation functions demonstrate the different types of NH-bond motion and order present in the peptide. The inset at the bottom right is an expanded time scale showing the initial decay of these same autocorrelation functions.

much more slowly fluctuating part. The autocorrelation function of the ninth residue decays very rapidly to a roughly constant value, whereas the autocorrelation function of the 21st residue consists, again, of a fast and a slow part. The slow decay of the autocorrelation function in the case of the two terminal lysine residues reflects the larger fluctuations at both ends of the peptide, whereas the residue in the bilayer center is in a stable α-helical conformation and is more highly ordered. More detailed analysis of θ_{NH} for different residues showed that the first three NH bond angles at the N-terminus were fluctuating over a relatively large range of angles, between 60° and 180°. This is a consequence of the fact that these hydrogens do not participate in intramolecular hydrogen bonds and therefore their motion is not restricted. The two lysine amide hydrogens at the C-terminus were involved in the hydrogen bonds stabilizing the α-helix; therefore the θ_{NH} bond angle motion was restricted to a narrower interval than at the N-terminus. As mentioned earlier, the leucine hydrogens 8–18 formed stable hydrogen bonds for at least 50% of the simulation time. Accordingly, the corresponding θ_{NH} angles did not have much motional freedom and were fluctuating about an average value of 160° with small rms deviations.

Motion of peptide side chains. It is believed that in many cases structural changes of proteins, including side-chain motions, are important for their activity (Brooks et al., 1988). Even though the peptide represents a simple model of a transmembrane α-helix, gaining an insight into the nature of the side-chain motions is useful for understanding more complex systems. The analysis focused on the motion of the leucine side chains, because the side chains of the lysines did not display a significant mobility. The distance between the terminal nitrogens N_ζ of lysine side chains was calculated at both termini from the trajectory. The average distance between N_ζ atoms of Lys^1 and Lys^2 was 13.9 ± 0.3 Å, indicating that the lysine chains were spread apart. The average distance between the N_ζ atoms of Lys^{20} and Lys^{21} was short, 3.9 ± 0.2 Å, implying that the two side chains are fairly close to each other, despite their positive charges.

The leucine side-chain motion was investigated in terms of the transitions of the χ_1 and χ_2 dihedral angles between their potential minima. The optimal rotamer values of both χ_1 and χ_2 angles correspond to 60° (*gauche*$^+$ state), −60° (*gauche*$^-$ state), and 180° (*trans* state). The state most frequently occupied by both χ_1 and χ_2 was *trans*, in which χ_1 and χ_2 spent 56.9% and 45.2% of the simulation time, respectively. The χ_1 angle spent the rest of the simulation in the *gauche*$^-$ state, with a relative occupancy of 43.1%. The *gauche*$^+$ state of χ_1 was not occupied, because of the steric clash of C^γ in position i and the carbonyl group in position $i - 3$ (Kovacs et al., 1995). On the other hand, the χ_2 angle was found in both *gauche*$^+$ and *gauche*$^-$ states, with 18.1% and 36.7% occupancy, respectively. The relative occupancies were calculated by averaging over all of the leucines and over the whole simulation.

The side chains of different leucines exhibit different degrees of mobility. A few characteristic examples of χ_1 and χ_2 behavior are shown in Fig. 9. Both dihedral angles of the Leu^7 side chain are practically immobile, whereas the side chain of Leu^{16} exhibits a significant mobility that is demonstrated by frequent transitions between potential minima. The side chain of Leu^{18} shows increased mobility toward the end of the simulation, with frequent transitions between *gauche*$^-$ and *trans* states. However, except for this case, no connection between the position of a side chain in the peptide and its mobility was noticed. To express the side-chain mobility in a quantitative manner, the average number of transitions of χ_1 and χ_2 angles was calculated. To distinguish a true transition from a large fluctuation, a transition was counted when a dihedral angle crossed the potential barrier and reached the bottom of the potential well (±5°) of the new conformation (Helfand, 1978). The time spent in a certain conformation was defined in accordance with this definition of a transition. The average transition rates were determined to be $6.2 \times 10^9\ s^{-1}$ for χ_1 and $11.2 \times 10^9\ s^{-1}$ for χ_2. The number of transitions ranged in both cases from two transitions over the whole simulation for Leu^7 to 27 transitions of χ_1 angle for Leu^{18}, and 27 transitions of χ_2 for Leu^{11}. The average occupancy times of all three potential minima were calculated from histograms with a bin width of 5 ps for both angles. The average lifetimes (i.e., the average times spent in particular states when they are occupied) of the χ_1 angle in the potential minima of −60° and 180° are 131 ps and 156 ps, respectively. The average lifetimes of the χ_2 angle in the potential

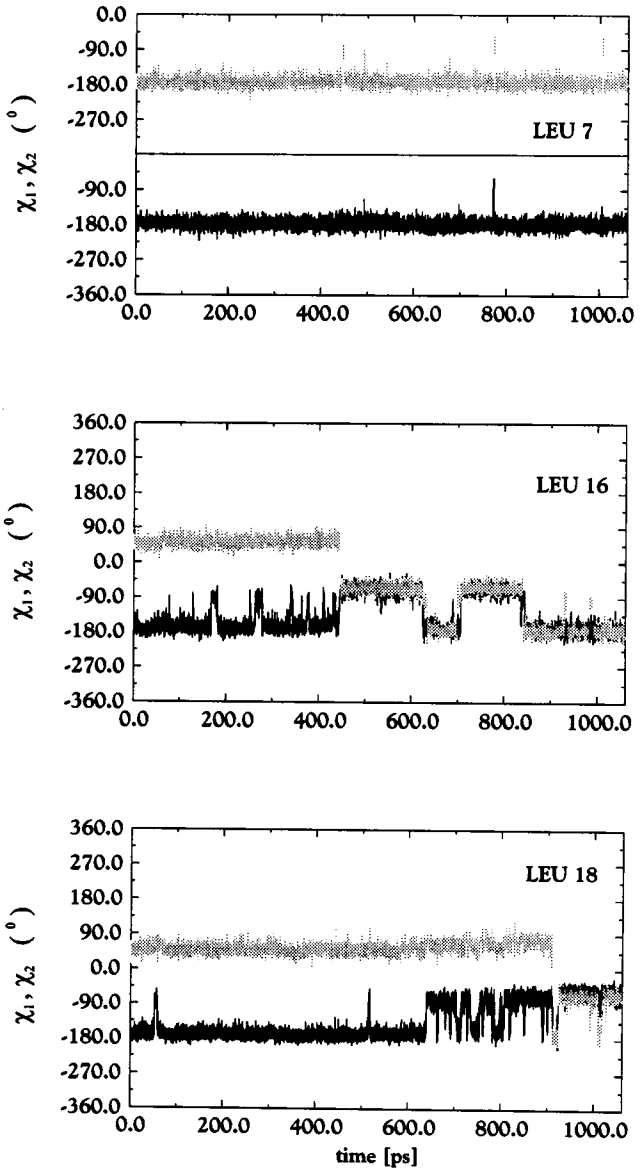

FIGURE 9 The motion of side chains of Leu[7], Leu[16], and Leu[18] is depicted in terms of the evolution of their respective χ_1 and χ_2 angles. The dark line represents the χ_1 angle and the light line represents the χ_2 angle.

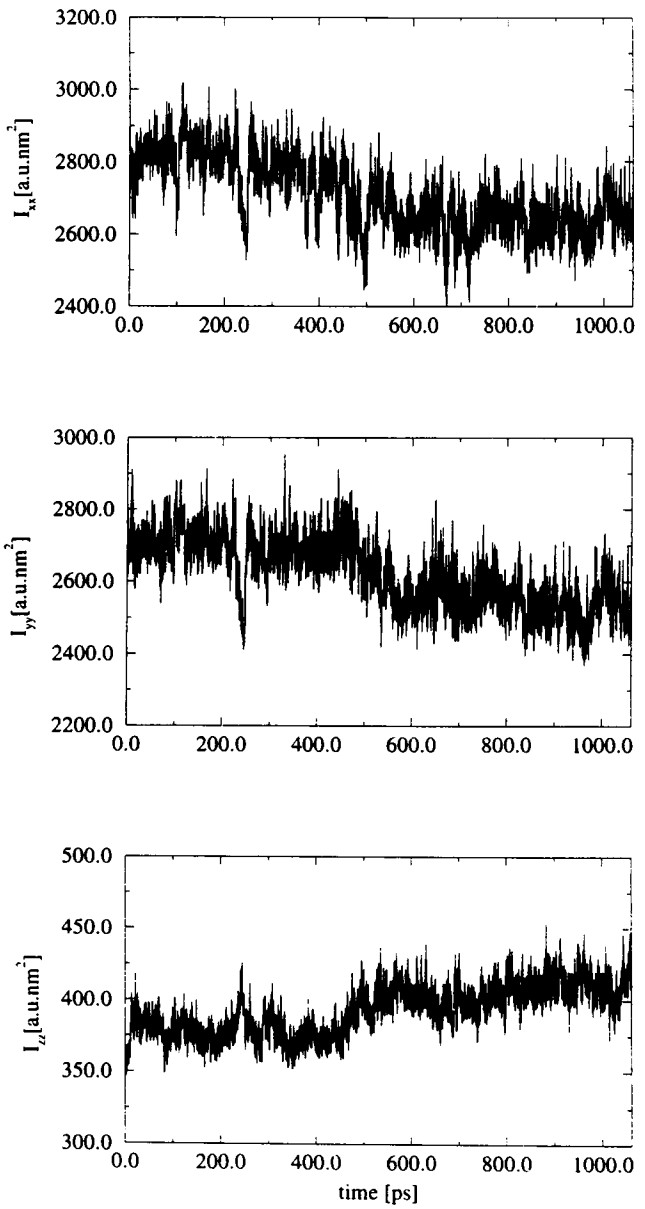

FIGURE 10 The evolution of the principal moments of inertia of the peptide.

minima of 60°, −60°, and 180° are 440 ps, 59.6 ps, and 70.5 ps. The average occupancy times (i.e., the average time spent in a particular state) of the χ_1 angle in the potential minima of −60° and 180° are 155.5 ps and 204.7 ps, respectively. The average occupancy times of the χ_2 angle in the potential minima of 60°, −60°, and 180° are 64.2 ps, 136.5 ps, and 165.9 ps. Thus the most probable state of both χ_1 and χ_2 dihedral angles appears to be the *trans* state.

Global peptide motions

The evolution of the principal moments of inertia I_{xx}, I_{yy}, and I_{zz} (see Fig. 10) illustrates changes of the peptide shape during the simulation. Because the helix axis is aligned with the z direction, I_{zz} is the smallest principal moment of inertia. I_{xx} and I_{yy} were determined so that the principal axes system would form a right-handed coordinate system. I_{xx} and I_{yy} are almost equal throughout the whole simulation, indicating that the molecule remains nearly axially symmetrical at all times. At ~250 ps changes in all three moments of inertia were observed, which were correlated with a temporary breakage of the $O_{12}H_{16}$ hydrogen bond. Later in the simulation, the helix underwent a slight deformation, beginning at ~500 ps. I_{xx} and I_{yy} decreased while I_{zz} increased, implying the shortening of the helix, whereas the cross-sectional area of the peptide became larger. However, the global helical shape remained unchanged, because I_{zz} was always the smallest principal moment of inertia, ac-

cording to Fig. 10. Taking the helix length as the distance between the centers of mass of the first helix turn and the last (i.e., sixth) helix turn, the evolution of this distance shows sudden changes that are correlated with the changes of principal moments of inertia. Later it will be shown that these changes in the helix length were caused by the deformation of the helix. As pointed out earlier, the deformation of the helix is likely to occur between Leu^{17} and Leu^{19}, because of a correlated change in the helix backbone dihedral angles at Leu^{16} and Leu^{17} at ~500 ps.

The global change in the helix conformation with respect to an ideal α-helix was assessed in terms of the rms difference between atom positions on the backbones of the two structures (the rms difference was obtained after reorienting the helix and overlapping it with the ideal α-helix). The evolution of the rms difference is illustrated in Fig. 11. It can be observed that for the first 10 ps, the rms difference fluctuated about 1.1 Å, then in the next 440 ps about 1.6 Å. In the following 60 ps, the rms difference gradually increased up to 2.1 Å, and it stayed there until the end of the simulation. This change occurred simultaneously with the conformational change between Leu^{16} and Leu^{17}.

Tilting and bending motions. During the simulation the peptide tilted with respect to the bilayer normal (Z axis). To investigate this type of motion, the angle between the helix axis and the bilayer normal was calculated (for its time dependence see Fig. 12). The angle fluctuates from 0° to ~26°, about an average value of 15.3°, with an rms deviation of 4.9°. For comparison, ^2H NMR relaxation studies of oriented multillamellar dispersions of DLPC and ^2H exchange-labeled gramicidin D (similar to the simulated system, in the sense that both peptides are small helical transmembrane peptides with an amphiphilic character) indicated that the rms angle formed by the peptide helix axes and the local bilayer normal was 16° ± 2° (Prosser and Davis, 1994). However, the simulation lasted for 1 ns, which is short compared to the slow time scale of the

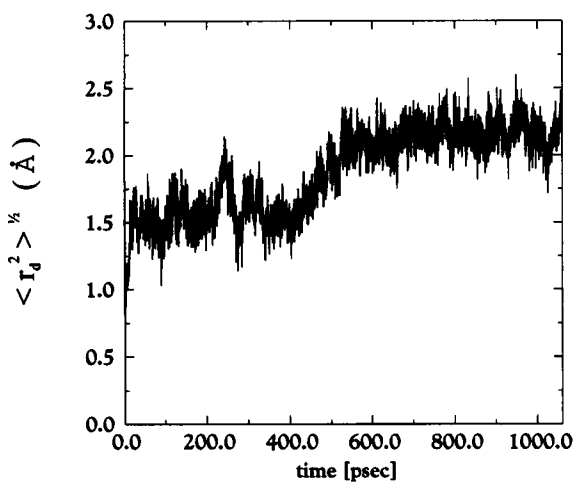

FIGURE 11 The evolution of the rms difference, $\langle rd^2 \rangle^{1/2}$, between the helix backbone and the ideal α-helix backbone.

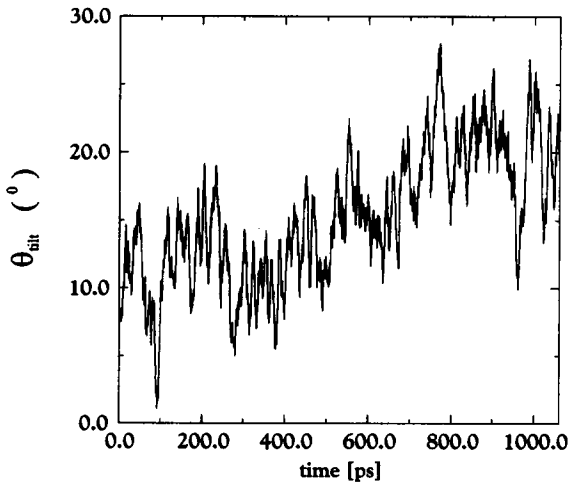

FIGURE 12 The evolution of the angle, θ_{tilt}, defining the tilt of the α-helix with respect to the bilayer normal. The angle was calculated as the angle between the helix axis and the bilayer normal.

"tilting" motion of the peptide. A much longer simulation would be required to quantitatively characterize this process. It is also worth noting that even though the thickness of the hydrophobic region of the bilayer (defined to be 22 Å thick; Lewis and Engelman, 1983) and the length of the hydrophobic core of the peptide (in an ideal α-helix corresponding to 24 Å) gave a very good match, the peptide tilted with respect to the bilayer normal.

Fig. 13 illustrates the difference between the peptide conformation at the end of the simulation and an ideal α-helix. It can be seen quite clearly that after more than 1 ns of equilibration and simulation, the helix is tilted with

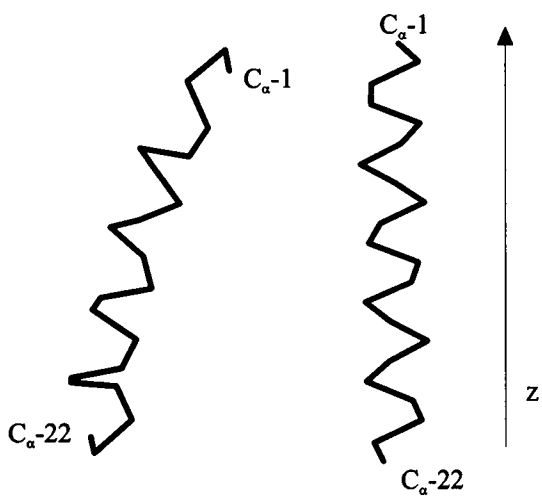

FIGURE 13 Comparison of the helix conformation at the end of the simulation (*on the left*) with respect to an ideal α-helix (*on the right*). It can be seen that at the end of the simulation, both helix termini were pointing toward the bilayer interior, whereas the helix was tilted with respect to the bilayer normal (the bilayer normal is parallel to the axis of an ideal α-helix on the right). Furthermore, the slight bend in the helix can be seen. It is evident that the N-terminus (the top of the helix) is unwound and extended.

respect to the bilayer normal (as was discussed in the previous section). Moreover, a very slight bend in the helix can be observed.

The bend in the helix was more closely analyzed by calculating the bend angle of the helix as the angle defined by the center of mass of the backbone atoms of the second turn (residues 4–7), the center of mass of the backbone atoms of the third turn (residues 8–11), and the center of mass of the backbone atoms of the fifth turn (residues 15–18). The turns 2, 3, and 5 were chosen because both the first and the last turns of the helix displayed a large degree of instability during the simulation. This would have biased the determination of the bend helix angle if they had been used in the definition. The motion of the centers of mass of the turns over the trajectory was calculated in the *xy* plane, and the centers of mass of the first and of the last turns sampled the largest region of the *xy* plane. The average value of the bend angle was determined to be 172°, with an rms deviation of 2.9°. This indicates a small bend in the helix with respect to a perfectly straight ideal α-helix. However, occasional excursions of the angle were observed, ranging up to 155°. To estimate contributions from the respective turns toward the total bend angle and to investigate the bend at both helix ends, the local bend angles were calculated. They were defined by the centers of mass of three consecutive turns. The largest fluctuations were observed at both ends of the helix, as expected. The most stable turns appeared to be turns 2, 3, 4, 5. The bend angle at the C-terminus assumed two different average values; in the first 500 ps of the simulation it fluctuated about 171.7° ± 4.3°. In the rest of the simulation it fluctuated about 144.4° ± 5.2°. The sudden change in the C-terminus conformation is exactly correlated with the breakage of $O_{15}H_{19}$ and $O_{16}H_{20}$ hydrogen bonds, and with the decrease in the distance between the centers of mass of the first and the last turns in the second half of the simulation. Thus the described end effect at the C-terminus has caused the shortening of the helix and consequently an increase in I_{zz}, the principal moment of inertia.

Even though the simulation is short (1 ns) compared to most experimental time scales, there was a variety of different peptide motions that can be divided into two groups. Local motions, occurring on a shorter time scale, such as the NH bond motion or the transitions of the peptide side chains between the potential minima, were sufficiently covered by the simulation. The whole-body molecular motions such as the tilt or bend of the peptide and the deformation of the peptide shape were probably not sampled sufficiently in the simulation. Another type of motion observed visually during the simulation was the axial diffusion of the peptide. However, this was not examined quantitatively, because of its long characteristic time.

Solvation of the peptide

Hydrophilic lysine side chains are located at both peptide termini, favorably close to the water interface. It is expected that the long and flexible chains are strongly interacting with the water region. To probe this assumption, the relative water solvation was analyzed by calculating the solvent radial distribution function of water oxygens about the peptide nonhydrogen atoms. The side-chain carbon atoms C_ϵ and N_ζ of all four lysines showed a formation of the first hydration shell, thus confirming the assumption that they were well hydrated. The shape of the distribution functions for apolar C_ϵ atoms was significantly broader than that of N_ζ, as observed by Brooks and Karplus (1989) in their molecular dynamics study of the active site of lysozyme. Even though the C-terminal lysines are located deeper in the lipid bilayer, their radial distribution functions were very similar. The terminal backbone atoms were not solvated significantly by water molecules, reflecting the fact that they were shielded from the aqueous phase by the side chains.

As was mentioned earlier, Leu^{17} 17 was hydrogen bonded to Lys^{21} for 12% of the simulation time. Therefore it was expected that its oxygen would be hydrogen bonded to water molecules throughout the rest of the simulation. The radial distribution function for oxygen of Leu^{17} indeed clearly shows a sharp peak at 2.7 Å (see Fig. 14 *a*). Minimum distances between every peptide oxygen and any water hydrogen, $d_{O\text{-}H}^{min}$, were calculated every 5 ps to see the evolution of the solvation of the peptide oxygens (a distance between a peptide oxygen and a water hydrogen of less than 2.5 Å indicates the possibility of a hydrogen bond). The evolution of the minimum distance between the oxygen of Leu^{17} and any water hydrogen, $d_{O17\text{-}H}^{min}$ (see Fig. 14 *b*), shows periods of time when the oxygen is possibly hydrogen bonded to water. As was discussed previously, the oxygen of Leu^{16} was free in the second half of the simulation (formation of the $i \rightarrow i + 5$ hydrogen bond was not seen, as in the case of the oxygen of Leu^{15}). From Fig. 14 *c* it was seen that it was occasionally bound to a water molecule. A closer inspection of water molecules around oxygens 16 and 17 showed that different water molecules were closer than 2.5 Å at different times in the simulation. Oxygens 20, 21, and 22 did not participate in the peptide intramolecular hydrogen bonds and remained hydrogen bonded to water molecules for most of the simulation. The first three oxygens at the N-terminus hydrogen bonded to water molecules for short periods of time. As discussed above, for part of the simulation they were participating in $i \rightarrow i + 3$ hydrogen bonds; however, for the rest of the simulation they were free, i.e., they were not hydrogen bonded to water or to the peptide amide hydrogens, which seems to be an energetically unfavorable situation.

In a similar fashion, the minimum distances between amide protons and any water oxygen were calculated. The first three amide protons at the N-terminus were hydrogen bonded to water oxygens during the last 660 ps of the simulation. Further analysis of the solvation of these amide protons was directed toward the investigation of their possible association with the lipid headgroup phosphoryl oxygens. The radial distribution functions of O_{13} (for the naming convention see Sundaralingam, 1972) of DMPC 11

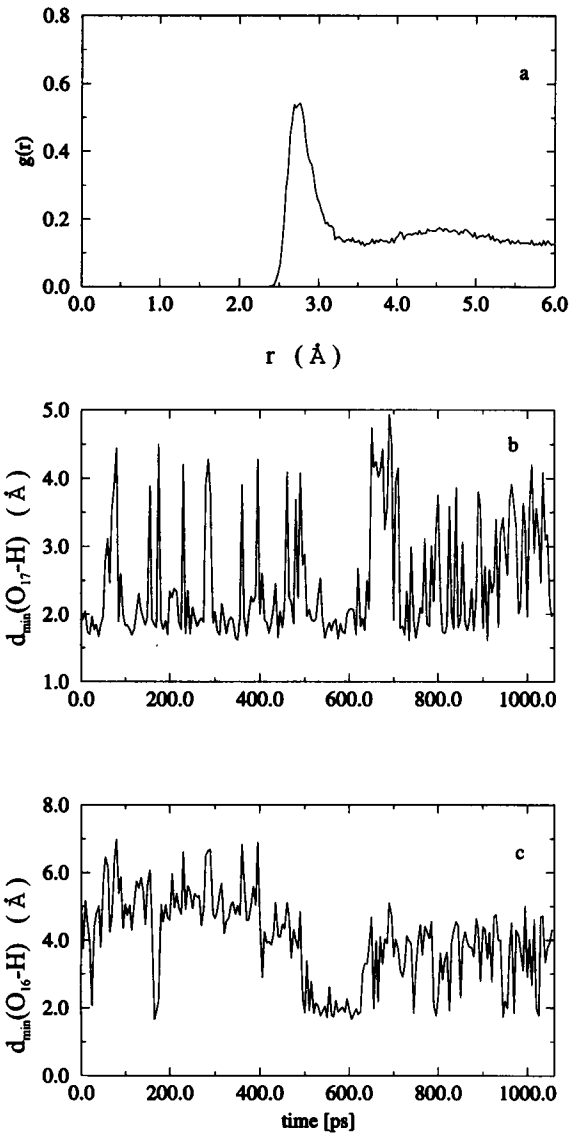

FIGURE 14 (*a*) The radial distribution function of water oxygens about the oxygen of Leu^{17}. (*b*) The minimum distance between the oxygen of Leu^{17} and any water hydrogen, $dO17\text{-}H^{min}$, sampled every 5 ps. (*c*) The minimum distance between the oxygen of Leu^{16} and any water hydrogen, $dO16\text{-}H^{min}$, sampled every 5 ps.

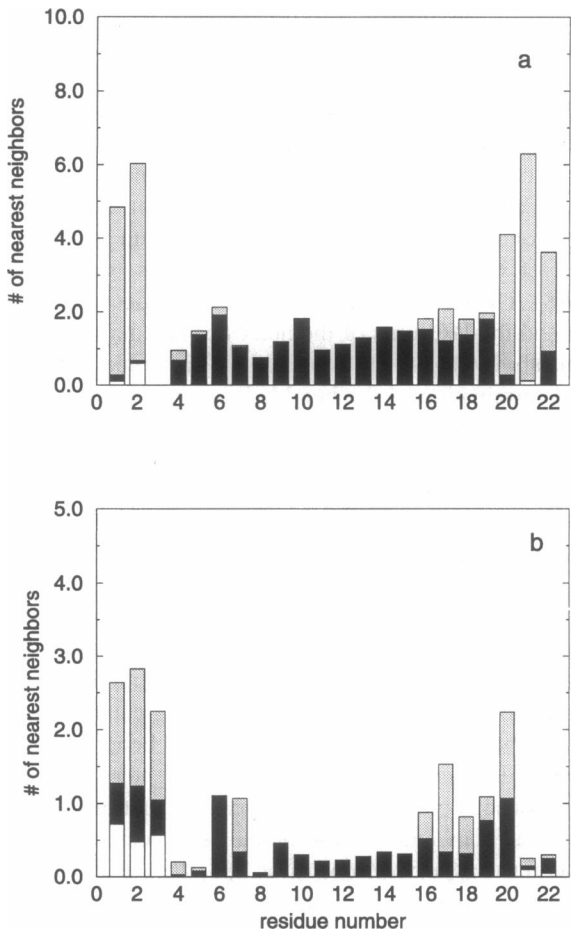

FIGURE 15 (*a*) The average number of near-neighbor atoms per side-chain atom within a distance of 4.5 Å around each side chain. (*b*) The average number of near-neighbor atoms per backbone atom within a distance of 4.5 Å around each backbone residue. White columns represent atoms in lipid phosphate groups, black columns represent hydrocarbon chains, and the grey columns represent water molecules.

about HN_1, HN_2, and HN_3 indicated a possible occurrence of hydrogen bonds between O_{13} and amide hydrogens. The distances between amide protons and a phosphoryl oxygen O_{13} of DMPC 11 were calculated, and these indicated that during the first 400 ps all three amide protons were hydrogen bonded to this oxygen atom for at least part of the time (HN_1 for 33.7% of the simulation, HN_2 for 18.2% of the simulation, and HN_3 for 21.5% of the simulation). It was shown earlier that the C-terminal amide protons participated in intramolecular hydrogen bonds, and the minimum distances between these amide protons and any water oxygens were greater than 2.5 Å for most of the simulation.

An overall picture of the peptide solvation can be obtained from Fig. 15, where the average number of water molecules, lipid phosphate groups, and lipid chains within a 4.5-Å distance of the peptide backbone atoms (Fig. 15 *a*) and of the peptide side-chain nonhydrogen atoms (Fig. 15 *b*) is displayed. It can be clearly seen that the backbone atoms were less solvated than the side chains, as noted previously. The backbone atoms at the N-terminus were less solvated than the backbone atoms at the C-terminus, with more contact with the phosphate groups and to the lipid chains. Backbone atoms of Leu^6 and Leu^{8-15} were in contact with hydrocarbon chains only. Some solvation of backbone atoms of Leu^{3-5}, Leu^7, and Leu^{16-19} was observed. The side chains at both termini exhibited a high degree of solvation by water molecules. The hydrophobic side chains of leucines were mainly in contact with hydrocarbon chains.

CONCLUSION

An MD simulation of a system composed of a synthetic peptide, acetyl-Lys_2-Gly-Leu_{16}-Lys_2-Ala-amide, and a fully

hydrated DMPC bilayer was carried out for 1060 ps. The initial configuration of the system was constructed using a protocol developed by Woolf and Roux (Woolf and Roux, 1996; Roux and Woolf, 1996). The calculated properties are characteristic of the system at the temperature of 336 ± 9 K. The primary points of interest in this simulation were the peptide's structural and dynamic properties. The analyzed structural properties of the peptide included the average backbone dihedral angles, the C_α torsion angles, the translation per residue along the helix axis, and the formation and duration of peptide intramolecular hydrogen bonds. On average, the peptide residues 6–15 and 18 stayed in the α-helical conformation, whereas both peptide ends exhibited more fluctuations. This finding agrees with experimental work showing the predominant secondary structure of peptide-*n* to be α-helical (Davis et al., 1983), and showing possible extensions of the peptide-*n* terminal residues (Zhang et al., 1992a). A long-lived disruption of the peptide structure between Leu^{16-19} observed midway through the simulation may have been initated by conformational change of the backbone dihedral angles ϕ and ψ of Leu^{16} and Leu^{17}. Consequently, the region of the helix between residues 17 and 19 was disrupted, and two regular intramolecular hydrogen bonds were lost.

The dynamics of the peptide involved local peptide motions, such as the NH bond dynamics and the side-chain dynamics, and global peptide motions, characterized by tilting and bending of the helix. The NH bond dynamics were analyzed in terms of the autocorrelation functions of the NH bond angles with respect to the helix axis. The autocorrelation times of residues at both termini differed from those in the stable portion of the peptide, because of a different degree of peptide "order" in these regions. The peptide exhibited considerable fluctuations at both peptide termini, whereas its hydrophobic core was stable. The motion of the side chains was investigated in terms of the transitions of χ_1 and χ_2 dihedral angles between their potential minima. All four lysine side chains were not very mobile, spending most of the simulation in one state. In contrast, the leucine side chains displayed a large variety of dihedral motions, from no large changes to frequent transitions between two or three potential minima. The most probable state for both χ_1 and χ_2 dihedral angles was the *trans* state. The evolution of the shape of the peptide was monitored, and it was observed that the overall shape of the helix remained virtually unchanged throughout the simulation. However, during the simulation the peptide became shorter and its cross-sectional area increased slightly. The evolution of the rms difference between the helix backbone and the ideal α-helix backbone confirmed that the backbone structure underwent a change after ~500 ps of the simulation. This is closely connected to changes in the backbone dihedral angles of Leu^{16} and Leu^{17}, which were correlated with the breakage of the hydrogen bonds and the deformation of helix region between residues 17 and 19. The global bend of the peptide was quantitatively defined as the angle determined by the centers of mass of the three helix turns, 2, 3, and 5. For most of the simulation it was very close to 180°, as expected for an ideal α-helix. When the unstable first and the last peptide turns were taken into account, we found that the helix underwent a significant bend in the second half of the simulation at the C-terminus. This bend in the helix produced the shortening and the slight changes in overall shape monitored by the three principal moments of inertia of the peptide. In addition to the bend in the helix, the peptide tilted with respect to the bilayer normal. The average tilt angle of the helical axis, calculated from the simulation, is similar to that deduced from NMR relaxation measurements on gramicidin D (Prosser and Davis, 1994) and to that of the simulation of an all-alanine α-helix in DMPC (Shen et al., 1997).

Analysis of the peptide solvation showed that lysine side chains extended to maximize their contact with the water phase, whereas the hydrophobic leucine side chains were mainly in contact with hydrocarbon lipid chains. The radial distribution function of water oxygens about the oxygen of Leu^{17} showed a first hydration shell. This indicated that some water molecules penetrated quite deeply into the hydrophobic region of the lipid bilayer. However, no water was observed to cross through the hydrophobic region of the bilayer from one side to the other.

Molecular dynamics simulations, such as the current trajectory, still cover a relatively short time compared to experiment. Nonetheless, the simulation provides a chance to closely examine the short time dynamics of the system. Even with this time limitation, valuable insights into the molecular behavior of complex systems may be obtained. The present investigation shows that the structure and dynamics of the transmembrane helix change according to the variations in the membrane environment. The α-helical backbone hydrogen bonds of the residues embedded in the hydrocarbon core are stable, whereas those near the membrane-bulk interface exhibit larger fluctuations. On the other hand, the leucine side chains buried in the nonpolar environment are more mobile than the solvated lysine side chains. Future work will explore the influence of the peptide on the structure and dynamics of the membrane.

The authors thank Prof. Bernie Nickel for many valuable discussions and the Natural Sciences and Engineering Research Council of Canada for financial support.

REFERENCES

Alper, H. E., and T. R. Stouch. 1995. Orientation and diffusion of a drug analogue in biomembranes: molecular dynamics simulations. *J. Phys. Chem.* 99:5724–5731.

Bassolino-Klimas, D., H. E. Alper, and T. R. Stouch. 1993. Solute diffusion in lipid bilayer membranes: an atomic level study. *Biochemistry.* 32:12624–12637.

Bassolino-Klimas, D., H. E. Alper, and T. R. Stouch. 1995. Mechanism of solute diffusion through lipid bilayer membranes by molecular dynamics simulation. *J. Am. Chem. Soc.* 117:4118–4129.

Brooks, B. R., R. E. Bruccoleri, B. D. Olafson, D. J. States, S. Swaminathan, and M. Karplus. 1983. CHARMM: a program for macromolec-

ular energy, minimization, and dynamics calculations. *J. Comput. Chem.* 4:187–217.

Brooks, C. L., and M. Karplus. 1989. Solvent effects on protein motion and protein effects on solvent motion. *J. Mol. Biol* 208:159–181.

Brooks, C. L., M. Karplus, and B. M. Pettitt. 1988. Proteins: A Theoretical Perspective of Dynamics, Structure and Thermodynamics. I. Prigogine and S. A. Rice, editors. Advances in Chemical Physics, Vol. LXXI. John Wiley and Sons, New York.

Cantor, C. R., and P. R. Schimmel. 1980. Biophysical Chemistry. Part I. The Conformations of Biological Macromolecules. W. H. Freeman and Co., San Francisco.

Creighton, T. E. 1983. Proteins: Structures and Molecular Principles. W. H. Freeman and Co., New York.

Damodaran, K. V., and K. M. Merz, Jr. 1995. Interaction of the fusion inhibiting peptide carbobenzoxy-D-Phe-L-Phe-Gly with *N*-methyldioleoylphosphatidylethanolamine lipid bilayers. *J. Am. Chem. Soc.* 117: 6561–6571.

Damodaran, K. V., K. M. Merz, Jr., and B. P. Gaber. 1995. Interaction of small peptides with lipid bilayers. *Biophys. J.* 69:1299–1308.

Davis, J. H., D. M. Clare, R. S. Hodges, and M. Bloom. 1983. Interaction of a synthetic amphiphilic polypeptide and lipids in a bilayer structure. *Biochemistry.* 22:5298–5305.

Deisenhofer, J., and H. Michel. 1989. The photosynthetic reaction center from the purple bacterium *Rhodopseudomonas viridis. Science.* 245: 1463–1473.

De Loof, H., S. C. Harvey, J. P. Segrest, and R. W. Pastor. 1991. Mean field stochastic boundary molecular dynamics simulation of a phospholipid in a membrane. *Biochemistry.* 30:2099–2113.

Dunbrack, R. L., and M. Karplus. 1993. Backbone-dependent rotamer library for proteins. Application to side-chain prediction. *J. Mol. Biol.* 230:543–574.

Edholm, O., O. Berger, and F. Jähnig. 1995. Structure and fluctuations of bacteriorhodopsin in the purple membrane: a molecular dynamics study. *J. Mol. Biol.* 250:94–111.

Edholm, O., and J. Johansson. 1987. Lipid bilayer polypeptide interactions studied by molecular dynamics simulation. *Eur. Biophys. J.* 14:203–209.

Ermler, U., G. Fritzsch, S. Buchanan, and H. Michel. 1992. *In* Research in Photosynthesis. N. Murata, editor. Kluwer, Dordrecht, the Netherlands. 341–347.

Gennis, R. B. 1989. Biomembranes: Molecular Structure and Function. Springer Verlag, New York.

Grigorieff, N., T. A. Ceska, K. H. Downing, J. M. Baldwin, and R. Henderson. 1996. Electron-crystallographic refinement of the structure of bacteriorhodopsin. *J. Mol. Biol.* 259:393–421.

Haile, J. M. 1992. Molecular Dynamics Simulations: Elementary Methods. John Wiley and Sons, New York.

Helfand, E. 1978. Brownian dynamics study of transitions in a polymer chain of bistable oscillators. *J. Chem. Phys.* 69:1010–1018.

Heller, H., M. Schaefer, and K. Schulten. 1993. Molecular dynamics simulation of a bilayer of 200 lipids in the gel and in the liquid-crystal phases. *J. Phys. Chem.* 97:8343–8360.

Hirst, J. D., and C. L. Brooks, III. 1995. Molecular dynamics of isolated helices of myoglobin. *Biochemistry.* 34:7614–7621.

Huang, P., and G. H. Loew. 1995. Interaction of an amphiphilic peptide with a phospholipid bilayer surface by molecular dynamics simulation study. *J. Biomol. Struct. Dyn.* 12:937–956.

Huschilt, J. C., B. Millman, and J. H. Davis. 1989. Orientation of α-helical peptides in a lipid bilayer. *Biochim. Biophys. Acta.* 979:139–141.

Jenkins, G. M., and D. G. Watts. 1968. Spectral Analysis and Its Applications. Holden-Day, San Fransisco.

Jorgensen, W. L. 1981. Quantum and statistical mechanical studies of liquids. 10. Transferable intermolecular potential functions for water, alcohols and ethers. Application to liquid water. *J. Am. Chem. Soc.* 103:335–345.

Jorgensen, W. L., J. Chandrasekhar, J. D. Madura, R. W. Impey, and M. L. Klein. 1983. Comparison of simple potential functions for simulating liquid water. *J. Chem. Phys.* 79:926–935.

Kovacs, H., A. E. Mark, J. Johansson, and W. F. van Gunsteren. 1995. The effect of environment on the stability of an integral membrane helix: molecular dynamics simulations of surfactant protein C in chloroform, methanol and water. *J. Mol. Biol.* 247:808–822.

Kühlbrandt, W., D. N. Wang, and Y. Fujiyoshi. 1994. Atomic model of plant light-harvesting complex by electron crystallography. *Nature.* 367: 614–621.

Langlais, D. B. 1994. Internuclear distance measurements using rotational resonance. Ph.D. thesis. University of Guelph, Guelph, Ontario, Canada.

Lewis, B. A., and D. M. Engelman. 1983. Lipid bilayer thickness varies linearly with acyl chain length in fluid phosphatidylcholine vesicles. *J. Mol. Biol.* 166:211–217.

Loncharich, R. J., B. R. Brooks, and R. W. Pastor. 1992. Langevin dynamics of peptides: the frictional dependence of isomerization rates of *N*-acetylalanyl-*N*-methylamide. *Biopolymers.* 32:523–535.

Mackerell, A. D., D. Bashford, M. Bellot, R. L. Dunbrack, M. J. Field, S. Fischer, J. Gao, H. Guo, D. Joseph, S. Ha, L. Kuchnir, K. Kuczera, F. T. K. Lau, C. Mattos, S. Michnick, D. T. Nguyen, T. Ngo, B. Prodhom, B. Roux, B. Schlenkrich, J. Smith, R. Stote, J. Straub, J. Wiorkiewicz-Kuczera, and M. Karplus. 1992. Self-consistent parametrization of biomolecules for molecular modelling and condensed phase simulations. *Biophys. J.* 61:A143.

Marrink, S. J., and H. J. C. Berendsen. 1994. Simulation of water transport through a lipid membrane. *J. Phys. Chem.* 98:4155–4168.

Mouritsen, O. G., and M. Bloom. 1993. Models of lipid-protein interactions in membranes. *Annu. Rev. Biophys. Biomol. Struct.* 22:145–171.

Nagle, J. F. 1993. Area/lipid of bilayers from NMR. *Biophys. J.* 64: 1476–1481.

Nezil, F. A., and M. Bloom. 1992. Combined influence of cholesterol and synthetic amphiphilic peptides upon bilayer thickness in model membranes. *Biophys. J.* 61:1176–1183.

Pastor, R. W. 1994. Molecular dynamics and Monte Carlo simulations of lipid bilayer. *Curr. Opin. Struct. Biol.* 4:486–492.

Pastor, R. W., and S. E. Feller. 1996. Time scales of lipid dynamics and molecular dynamics. *In* Biological Membranes: A Molecular Perspective from Computation and Experiment. K. M. Merz, Jr., and B. Roux, editors. Birkhäuser, Boston. 3–29.

Pastor, R. W., R. H. Venable, and M. Karplus. 1991. Model for the structure of the lipid bilayers. *Proc. Natl. Acad. Sci. USA.* 88:892–896.

Pauling, L., and R. B. Corey. 1951. The structure of synthetic polypeptides. *Proc. Natl. Acad. Sci. USA.* 37:241–250.

Pauls, K. P., A. L. MacKay, O. Söderman, M. Bloom, A. K. Tanjea, and R. S. Hodges. 1985. Dynamics properties of the backbone of an integral membrane polypeptide measured by ^{2}H-NMR. *Eur. Biophys. J.* 12:1–11.

Picot, D., P. J. Loll, and R. M. Garavito. 1994. The X-ray structure of the membrane protein prostaglandin H2 synthase-1. *J. Mol. Biol.* 227: 493–509.

Prosser, R. S., and J. H. Davis. 1994. Dynamics of an integral membrane protein: a deuterium NMR relaxation study of gramicidin. *Biophys. J.* 66:1429–1440.

Prosser, R. S., J. H. Davis, C. Mayer, K. Weisz, and G. Kothe. 1992. Deuterium NMR relaxation studies of peptide-lipid interactions. *Biochemistry.* 31:9355–9363.

Ramakrishnan, C., and K. V. Soman. 1982. Identification of secondary structures in globular proteins—a new algorithm. *Int. J. Pept. Protein Res.* 20:218–237.

Roux, B., and T. B. Woolf. 1996. Molecular dynamics of Pf1 coat protein in a phospholipid bilayer. *In* Biological Membranes: A Molecular Perspective from Computation and Experiment. K. M. Merz, Jr., and B. Roux, editors. Birkhäuser, Boston. 555–587.

Ryckaert, J.-P., G. Ciccotti, and H. J. C. Berendsen. 1977. Numerical integration of the Cartesian equations of motion of a system with constraints: molecular dynamics of *n*-alkanes. *J. Comput. Phys.* 23: 327–341.

Shen, L., D. Bassolino, and T. Stouch. 1997. Structure and interaction of a transmembrane polyalanine alpha-helix with a DMPC bilayer studied by multi-nanosecond molecular dynamics simulation. *Biophys. J.* 73:3–20.

Song, L., M. R. Hobaugh, C. Shustak, S. Cheley, H. Bayley, and J. E. Gouaux. 1996. Structure of staphylococcal α-hemolysin, a heptameric transmembrane pore. *Science.* 274:1859–1866.

Stouch, T. R. 1993. Lipid membrane structure and dynamics studied by all-atom molecular dynamics simulations of hydrated phospholipid bilayers. *Mol. Sim.* 10:335–362.

Stowell, M. H. B., and D. C. Rees. 1995. Structure and stability of membrane proteins. *Adv. Protein Chem.* 46:279–311.

Sundaralingam, M. 1972. Molecular structures and conformations of the phospholipids and sphingomyelins. *Ann. N.Y. Acad. Sci.* 195:324–355.

van Gunsteren, W. F., P. H. Hünenberger, A. E. Mark, P. E. Smith, and I. G. Tironi. 1995. Computer simulation of protein motion. *Comput. Phys. Commun.* 91:305–319.

van Gunsteren, W. F., and A. E. Mark. 1992. On the interpretation of biochemical data by molecular dynamics computer simulation. *Eur. J. Biochem.* 204:947–961.

Venable, R. M., Y. Zhang, B. J. Hardy, and R. W. Pastor. 1993. Molecular dynamics simulations of a lipid bilayer and of hexadecane: an investigation of membrane fluidity. *Science.* 262:223–226.

Verlet, L. 1967. Computer experiments on classical fluids. I. Thermodynamical properties of Lennard-Jones molecules. *Phys. Rev.* 159:98–103.

Weiss, M. S., and G. E. Schulz. 1992. Structure of porin refined at 1.8 angstroms resolution. *Nature.* 367:243–249.

Woolf, T. B. 1996. Molecular dynamics simulations of individual bacteriorhodopsin helices in explicit DMPC. *Biophys. J.* 70:A377.

Woolf, T. B., and B. Roux. 1994a. Molecular dynamics simulation of the gramicidin channel in a phospholipid bilayer. *Proc. Natl. Acad. Sci. USA.* 91:11631–11635.

Woolf, T. B., and B. Roux. 1994b. Conformational flexibility of *o*-phosphorylcholine and *o*-phosphorylethanolamine: a molecular dynamics study of solvation effects. *J. Am. Chem. Soc.* 116:5916–5926.

Woolf, T. B., and B. Roux. 1996. Structure, energetics and dynamics of lipid-protein interactions: a molecular dynamics study of the gramicidin A channel in a DMPC bilayer. *Proteins.* 24:92–114.

Zhang, Y. P., R. N. A. H. Lewis, R. S. Hodges, and R. N. McElhaney. 1992a. FTIR spectroscopic studies of the conformation and amide hydrogen exchange of a peptide model of the hydrophobic transmembrane α-helices of membrane proteins. *Biochemistry.* 31:11572–11578.

Zhang, Y. P., R. N. A. H. Lewis, R. S. Hodges, and R. N. McElhaney. 1992b. Interaction of a peptide model of a hydrophobic transmembrane α-helical segment of a membrane protein with phosphatidylcholine bilayers: differential scanning calorimetric and FTIR spectroscopic studies. *Biochemistry.* 31:11579–11588.